ELSEVIER

Ceramics International 25 (1999) 497–504

CERAMICS INTERNATIONAL

Thermal fatigue of alumina: comparison with mechanical data and life time prediction

M. Saadaoui [a,*], C. Olagnon [b], G. Fantozzi [b]

[a] *Ecole Mohammadia d'Ingénieurs, B.P. 765, Agdal, Rabat, Morocco*
[b] *INSA-GEMPPM, UMR 5510, 69621 Villeurbanne Cedex, France*

Received 24 March 1997; accepted 9 September 1997

Abstract

The thermal fatigue behaviour of a fine and a coarse grain alumina ceramics were investigated both experimentally, via an instrumented thermal shock apparatus, and analytically. Indented rectangular specimens were thermally cycled at an applied temperature difference ΔT. The determination of the subcritical crack growth law responsible for the thermal fatigue was deduced from the plot of the critical cycle number versus the initial crack size. The comparison of this result to the subcritical crack growth behaviour obtained from isothermal mechanical test reveals that some cyclic effects are present and life time therefore can not be predicted from the simple mechanical results. Calculation of the crack propagation using the thermal fatigue law is in rather fair agreement with the experiment for the fine grain material.

1. Introduction

Thermal fatigue, i.e. fatigue caused by a thermally induced stress, is an important property that can seriously limit the life time of components. Conversely to thermal shock, it has not been intensively studied owing to the inherent difficulties met in the assessment. Like most fatigue tests, a significant problem is the result scattering that induces the need of a large number of experiments. A related difficulty is the long duration of a thermal cycle, especially when compared to mechanical fatigue. In addition, the precise stress field is difficult to evaluate because of its transient nature and the number of parameters involved.

Thermal fatigue experiments are generally conducted by heating up a specimen and subsequently quenching it. The damage is recorded as a function of the number of cycle. Most of the thermal fatigue analyses [1] have been achieved by considering that damage is a thermal stress induced subcritical crack growth phenomena. A standard power law is therefore pre-supposed and the crack velocity is integrated over the different cycles up to the critical cycle number, corresponding to unstable crack propagation. This result shows that the logarithm plot of the critical cycle number as a function of the temperature difference (i.e. the maximum temperature difference occurring during one cycle) should define a straight line from which the parameters of the subcritical crack growth law could be determined. The first results published by Hasselman on glass showed a significant trend but associated with a large dispersion. Different solutions have been proposed to overcome these difficulties related to scattering. Hasselman et al. [2] were testing nine specimens simultaneously but they stopped the test when the first five specimens were broken. The critical cycle number of the fifth specimen was considered as the average value. Kamiya and Kamigaito [3] have applied a Weibull statistics to analyze their results. The analysis leads to the representation of the loglog of the failure probability vs the log of the critical cycle number.

Singh et al. [4] have proposed a modified analysis that takes into account the temperature dependence that has been applied by Glandus and Simoneau [5]. In principle, the different parameters could be obtained by different series of tests but the scattering was large. Sudreau et al. [6] have proposed a statistical approach which consists of relating the distribution of defect sizes to the critical cycle number distribution, by means of the pre-supposed propagation law. The parameter are obtained by fitting the results to the theoretical law.

* Corresponding author.

0272-8842/99/$ - see front matter
PII: S0272-8842(97)00084-9

Most of these analyses could not lead to the full determination of the crack law in the condition of thermal fatigue since several parameters could not be accurately determined.

Fett et al. [7] have made a detailed analysis of thermal fatigue on glass at moderate temperature. They have successfully compared experimental results to a fracture mechanics analysis made with mechanical measurements of subcritical crack growth. Magerl et al. [8] have conducted thermal cycles on a specific system where the thermal stress is induced by quasi-static temperature profile. This allowed them to derive the subcritical crack growth law under static and cycling thermal stress, which showed that for a 20% SiC–Al_2O_3 composite a cycling effect did exist while was not present for a HIP-RBSN. Olagnon et al. [9] have compared crack propagation obtained from thermal fatigue and from static double torsion test for a Mg-PSZ ceramic. The observed discrepency was attributed to cyclic effects.

For glass or dense ceramics the sample damage is obtained when a fast fracture occurs. For more complicate microstructure materials, alternative thermal fatigue damage accumulation have been considered. Case et al. [10] have recorded the Young modulus variation of SiC whisker reinforced alumina as a function of the thermal cycles. Konsztowicz [11] has recorded the acoustic emission as function of thermal cycles.

The aim of the present work was to show that thermal fatigue can be predicted from mechanical tests. For this purpose the crack propagation behaviour of two different aluminas has been evaluated by thermal fatigue, and double torsion under static and cyclic loading. Finally a simulation is conducted from the propagation law obtained under thermal fatigue regime.

2. Analysis

In general, the thermal fatigue behaviour of a brittle material is investigated by determining the critical number of thermal cycles, N_c, required to cause failure of specimens cycled over a range of applied temperature differences ΔT. The crack growth law necessary for life time predictions is determined from a thermal fatigue curve representing the plot of N_c vs ΔT. In this study, a set of specimens containing controlled flaws is thermally cycled applying the same temperature difference ΔT. The analysis is based on the works of Kamiya and Kamigaito [3] and Hasselman [1] who considered that thermal fatigue is due to subcritical crack extension under thermally induced stresses. The crack growth rate dc/dt, can generally be expressed as a power function of the stress intensity factor (SIF) K_I:

$$\frac{dc}{dt} = AK_I^n \tag{1}$$

where A and n are constants that depend on the material and environment. K_I is defined by:

$$K_I = \sigma_{th} \cdot Y \cdot \sqrt{c} \tag{2}$$

where σ_{th} is a stress characteristic of the thermal effects and generally the maximum stress at the specimen surface, c is the size of a crack in the specimen, and Y is a configuration coefficient dependent on the shape of the crack and the sample.

σ_{th} which depends both on time and temperature is generally expressed as the product of the applied temperature difference ΔT to a function of time, $f(t)$:

$$\sigma_{th} = \Delta T \cdot f(t) \tag{3}$$

By combining Eq. (3) with (2) and (1) the differential equation describing the crack propagation [Eq. (1)] can be rewritten as:

$$\frac{dc}{dt} = A \cdot \Delta T^n \cdot f^n \cdot (t) \cdot Y^n \cdot c^{n/2} \tag{4}$$

Assuming Y to be constant, the integration of Eq. (4) over the total crack extension leads to:

$$\frac{2}{2-n}\left[c^{\frac{2-n}{2}}\right]_{c_i}^{c_f} = A \cdot \Delta T^n \cdot Y^n \cdot N_c \int_0^{t_c} f^n(t) \cdot dt \tag{5}$$

with c_i initial crack size, c_f final crack size and t_c cycle duration.

Generally, $c_f^{-n} \ll c_i^{-n}$, thus Eq. (5) can be simplified to:

$$(c_i)^{\frac{2-n}{2}} = \frac{n-2}{2} \cdot N_c \cdot A \cdot \Delta T^n \cdot Y^n \cdot \int_0^{t_c} f^n(t) \cdot dt \tag{6}$$

Generally, the crack growth parameters are determined from the slope and the position of the straight line fitting the logarithmic plot of the critical cycle number versus the applied temperature difference. However, owing to the life time scattering the precision is poor. In this study, the expression (6) is used with different variables: the initial crack size c_i and the critical cycle number N_c. The plot of $\log(N_c)$ vs $\log(c_i)$ can be fitted by a straight line of slope equal to $(2/n-2)$, which gives the exponent n of the power law. The A parameter can also be calculated after the evaluation of the thermal stress σ_{th} and the configuration coefficient Y.

3. Experiments

3.1. Materials and samples

Two alumina ceramics were used for this study. The first one denoted A3 is an homogenous fine grain material with an average grain size of 3 μm, obtained by sintering at 1550°C for 2 h a high purity (>99.9) powder

(SM8 Baikowski). The second material denoted A25 is a commercial alumina (AF997, Desmarquest), characterized by an average grain size of 25 μm.

The thermal fatigue experiments were carried out on rectangular bars ($3\times4\times40\,mm^3$) with controlled indentation flaws. The largest face of each specimen was polished to a 1 μm finish using diamond paste, and the samples were annealed at 1300°C for 2 h to release any machining residual stresses. A Vickers indentation was made in the center of the polished surface with its diagonals aligned parallel to the specimen edges. Several indentation loads were used, from 30 to 50 N for the A3 material and from 100 to 150 N for the A25 material. The residual stresses generated by the indentation were relaxed by an annealing heat treatment of the samples at 1300°C for 2 h. The length of the surface radial crack, $2c$, was measured by optical microscopy.

3.2. Thermal loading

Cyclic thermal shock tests were performed using the apparatus details that have been previously described in Ref. [12]. The indented specimens were heated in a resistance furnace for 10 min and cooled symmetrically by the application of two jets of pulsed air at ambient temperature to the largest faces. The same temperature difference $\Delta T = 830 \pm 2°C$ was applied to the samples of both materials.

The surface heat transfer coefficient measured on the frontal and the lateral faces of the specimen [12] has the same value $h = 600\ W\ m^{-2}K^{-1}$.

The acoustic emission (AE) of the sample was monitored by a piezoelectric transducer connected to a wave guide in contact with the specimen. The acoustic emission during the first 6 seconds of cooling was recorded, allowing the determination of the critical cycle number N_c, for which one peak corresponding to unstable crack propagation was detected. It is important to note that only the unstable crack propagation could be recorded. The experiment was stopped after 600 cycles if no AE signal was detected.

4. Subcritical crack growth

The subcritical crack growth (SCG) was investigated under isothermal static loading for comparison with the thermal fatigue behaviour. Double torsion (DT) [13] and dynamic fatigue in bending [14] methods were used to calculate the parameters A and n of the crack growth relation $dc/dt = AK_I^n$. The double torsion (DT) experiments were performed on the fine grain material A3 in air at room temperature and at 800°C. The relaxation method [13] was applied to samples ($2\times20\times40$ mm) without guiding groove. Cyclic loading tests were also performed on precracked double torsion specimens with a constant frequency of 1 Hz. Sinusoidal loading was applied with various amplitudes and a constant minimal value of 10 N. The crack growth rate was determined as described in Ref. 15 as a function of the maximum applied stress intensity factor (SIF) during the cycling.

The crack propagation curves are shown in Fig. 1 and the corresponding values of the parameters A and n are displayed in Table 1 with two stages for the static loading tests. It can be seen that the n value under cyclic loading is much lower than under static loading which indicates cyclic fatigue effects.

The crack growth relation was also calculated from the experimental data of the dynamic fatigue method (constant loading rate) in bending performed at 800°C, using indented specimens identical to those used for thermal tests. The crack size chosen close to those used for the thermal tests is about 95 μm for the A3 alumina and about 200 μm for the A25 material. The results are represented in Fig. 2 as the plot of the fracture strength σ_f, vs the loading rates $d\sigma/dt$ in the range of 0.02 to 1000 MPa s^{-1}. The SCG parameters were determined from the straight line fitting the $\log\sigma_f$– $\log(d\sigma/dt)$ data according to the relation [16]:

$$(\sigma_f)^{n+1} = \left[\frac{2(n+1)}{(n-2)AY^n}(c_i)^{\frac{2-n}{2}}\right].\frac{d\sigma}{dt} \quad (7)$$

where c_i denotes the initial crack size and Y is a configuration coefficient.

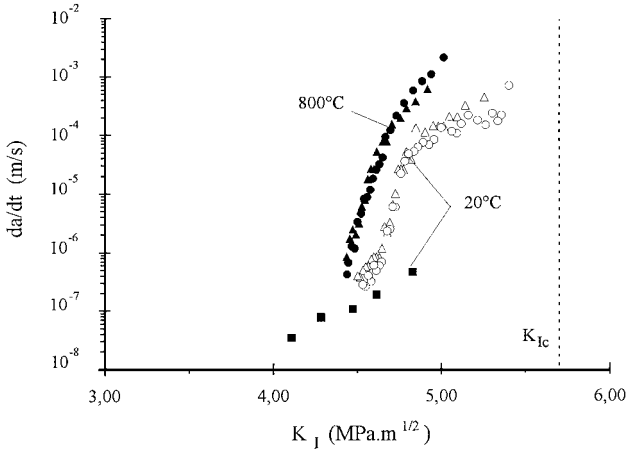

Fig. 1. Crack growth rate vs SIF for the A3 alumina from DT method. The solid squares represent cyclic loading data.

Table 1
SCG parameters from the DT method for the A3 alumina

	Stage 1		Stage 2	
Temperature	n_1	$\log(A_1)$	$n2$	$\log(A_2)$
20°C, static	87	−71	12	−12.5
800°C, static	76	−55	38	−29
20°C, cyclic	14	−16.5	—	—

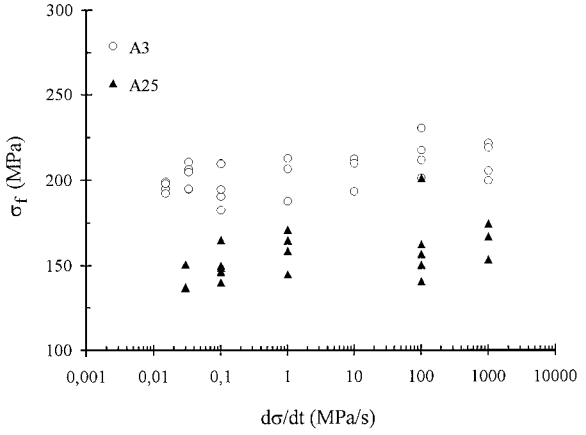

Fig. 2. Fracture strength vs the stressing rate in the dynamic fatigue bending tests.

Note the high n value obtained for the A3 material compared with that calculated from DT experiment at the same temperature (Table 1). This may be attributed to the difference between the cracks used in the two methods: DT specimens contain macro-cracks of several millimetres long whereas small cracks are used in the dynamic bending method.

5. Thermal fatigue results

5.1. Crack growth law

Detailed examination of the tested specimens showed that only the indentation cracks running parallel to the longitudinal direction of the specimen had propagated. The thermal fatigue results are represented in Fig. 3 in terms of the critical cycle number as a function of the initial surface crack size c_i. The open symbols represent the specimens for which no crack propagation occurred after 600 cycles. In spite of the significant scattering and the very steep slope, one can note the general trend for the critical cycle number to decrease with increasing crack size. Above a limit value of the initial crack size

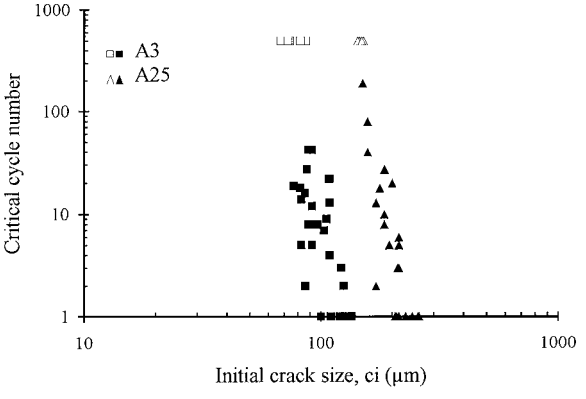

Fig. 3. Critical thermal cycle number vs the initial crack size.

Table 2
SCG parameters from dynamic fatigue tests at 800 °C

Material	n	A
A3	137	1.9×10^{-60}
A25	76	5.7×10^{-36}

equal to 120 and 250 μm for A3 and A25, respectively, unstable crack propagation occurs during the first cycle indicating that the toughness of the material is reached for those crack sizes.

The plot of $\log(N_c)$ vs $\log(c_i)$ is fitted by a straight line of slope $(2/n-2)$ from which n values of about 18 and 24 for the A3 and the A25 materials, respectively, were evaluated. The crack sizes for which the unstable crack growth occurs systematically at the first cycle were not taken into account.

Determination of the A parameter requires the knowledge of the thermal stress and the configuration coefficient Y. The transient stress induced during a thermal cycle has been evaluated by finite element as it has been previously described [17], taking into account the variations with temperature of the physical and elastic properties of the material. The maximum normal stress arises at the intercept of the crack plane with the surface of the sample. Therefore, only this component which induces mode I propagation of the surface crack is considered. Fig. 4 shows the variation with time of this surface stress as calculated by finite element. This result has been fitted to the following expression, which allowed numerical evaluation of the integral in Eq. (7):

$$\sigma_{th}(t) = \Delta T \cdot \left[\alpha \cdot \sqrt{t} \cdot \exp\left(\frac{t^{\beta}}{\gamma}\right)\right] \tag{8}$$

α, β, and γ are, respectively, equal (SI) to $12{,}7.10^{-3}$, 0.98 and -1570 for A3, and to $12{,}5.10^{-3}$, 0.948 and -1065 for the A25 alumina.

In order to investigate the crack shape evolution, necessary to determine the configuration coefficient Y, some of the tested specimens of the fine grain material

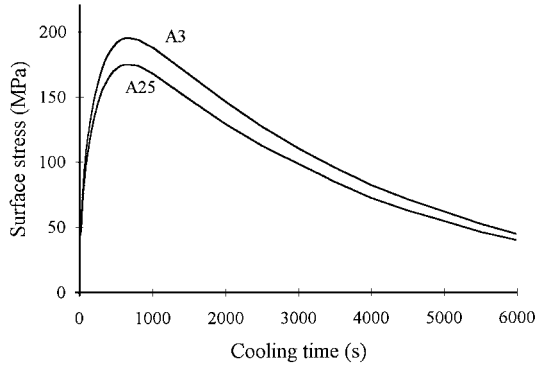

Fig. 4. Surface stress evolution during the cooling phase of a thermal cycle.

were subsequently broken along the crack plane. The crack arrest marks allowed the measurement of the final crack sizes. The crack front initially semi-circular takes a semi-elliptic shape where the ratio of the minor axis a_f (depth), to the major axis c_f (surface), is between 0.42 and 0.63 (Table 3).

As a consequence of the crack shape variation, the configuration coefficient Y decreases during crack extension as it depends on both the crack depth a and the aspect ratio a/c. In order to take into account this variation, the lowest and the highest values of Y denoted by Y_{min} and Y_{max}, respectively have been calculated for the investigated range of the crack sizes. For this purpose, the thermally induced SIF has first been numerically calculated (for details see Ref. [17]) and the Y values were subsequently evaluated using Eq. (2), in which σ_{th} was taken as the maximum surface stress. Y_{max} have been derived from the lowest initial crack size (for which $a/c = 1$) and the maximum of the stress intensity factor thermally induced for this crack size. Y_{min} have been calculated considering the final crack sizes measured on the fracture surface and the stress intensity factors determined under thermal loading at the instant of unstable crack growth.

For the coarse grained alumina A25, the final crack shapes could not be investigated owing to the important rugosity of the fracture surface, so Y_{min} have been taken identical to that obtained for the A3 material.

Y_{min} and Y_{max} have been used to determine the limiting values of the parameter A, respectively A_{max} and A_{min} according to the expression:

$$A = \frac{2B}{(n-2)\cdot Y^n \cdot I_n} \tag{9}$$

where log B is the ordinate of the intercept of the straight line fitting log(N_c) vs log (c_i) data (Fig. 3) with the log(Nc) axis, and I_n is defined by:

$$I_n = \Delta T^n \cdot \int_0^{t_c} f(t)^n \cdot dt \tag{10}$$

Table 3
Initial and final crack sizes for the A3 material

c_i(μm)	a_f(μm)	c_f(μm)	a_f/c_f
76	256	611	0.42
79	189	389	0.49
82	289	500	0.58
85	267	556	0.48
85	224	389	0.63
88	233	522	0.45
91	200	422	0.47
91	222	389	0.57
91	300	500	0.60
108	278	444	0.63
108	233	456	0.51
121	267	500	0.53

The results obtained for the two aluminas are reported in the Table 4. Notice that the n values are lower than those corresponding to monotonic mechanical loading. For the A3 material, the n value under thermal condition is close to that obtained under double torsion cyclic loading (Table 1).

5.2. Comparison with the mechanical results

The crack growth laws obtained under thermal and mechanical loading are compared in Fig. 5 and Fig. 6 for the A3 and the A25 aluminas respectively. The results are plotted as the crack growth rate vs the ratio

Table 4
Crack growth parameters under thermal fatigue

Material	n	Y_{min}	Y_{max}	logA_{max}	logA_{min}
A3	18	0.8	1.2	−11.8	−15
A25	24	0.8	1.16	−13.7	−17.6

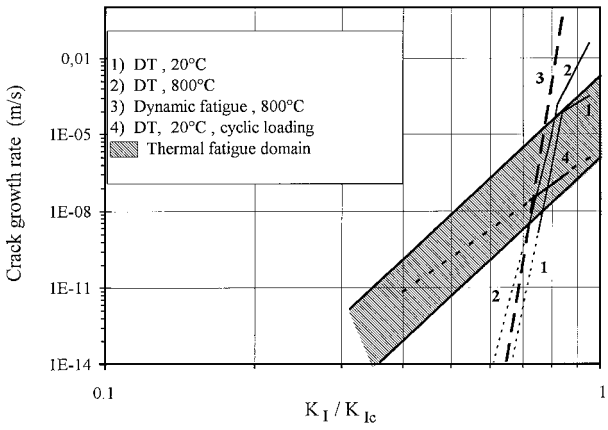

Fig. 5. Comparison of the thermal fatigue domain to the subcritical crack growth laws obtained under mechanical loading of the A3 alumina.

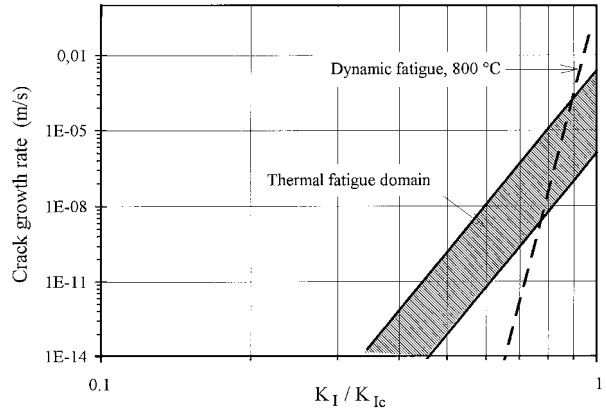

Fig. 6. Comparison of the thermal and the dynamic fatigue results for the A25 alumina.

of the SIF K_I to the toughness of the material K_{Ic}, determined for each testing conditions. For the thermal fatigue experiments the toughness was calculated considering the smallest initial crack for which the unstable crack propagation occurred at the first cycle. The stress intensity factor was calculated at the surface point of this crack at the instant of the unstable crack growth determined from the acoustic emission response; details of the calculation are given in Ref. [17]. Toughness values of 3.2 and 2.9 MPa $m^{1/2}$ were obtained for A3 and A25 aluminas, respectively.

It can be seen from Figs. 5 and 6 that the crack growth rate under thermal loading is higher than under static isothermal loading within a large domain of SIF. The crack growth rate corresponding to cyclic loading of DT specimens is close to the lower limit of the thermal fatigue. Those results clearly show that the life time prediction under thermal fatigue cannot be made simply from a SCG law obtained from either static mechanical or cyclic room temperature tests. Both cyclic effects and temperature variation must be taken into account.

6. Analysis of the crack growth

The objective of this part is to predict the crack growth found in the thermal fatigue experiments by a numerical simulation based on fracture mechanical analysis. A flow diagram that describes the calculation procedure is represented in Fig. 7. The indentation crack initially semi circular takes the shape of a semi-ellipse of depth a and length $2c$. The crack extensions Δa at the deepest point A of the crack and Δc at the surface point C are calculated over one loading cycle. To take into account the stress variation, the duration of the cooling phase of a thermal cycle (6s) is divided into small elements dt as follows:

$dt = 20$ ms for $t \leq 100$ ms;
$dt = 50$ ms for 100 ms $< t \leq 700$ ms;
$dt = 100$ ms for 700 ms $< t \leq 1500$ ms;
$dt = 500$ ms for 1500 ms $< t \leq 6000$ ms.

The average stress intensity factors K_A and K_C, are calculated at point A and C, respectively, using the weight function method as described in Ref. 17. For this purpose, the temperature distribution and the resulting transient stresses in the uncracked sample are calculated by finite element taking into account the variation with the temperature of the material properties and the measured value of the surface heat transfer coefficient.

For each time increment dt the crack propagation law is applied at A and C as

$$da = A(K_A)^n dt \tag{11a}$$

$$dc = A(K_C)^n dt \tag{11b}$$

The new crack sizes $(a + da)$ and $(c + dc)$ are introduced again into Eq. (11) to calculate the crack extension during the next time step. At the end of the cooling duration, the total crack increments during one cycle Δa and Δc are obtained, and the procedure is repeated until K_A or K_C reaches the toughness of the material calculated under thermal loading (3.2 MPa.$m^{1/2}$ and 2.9 MPa $m^{1/2}$ for A3 and A25 respectively).

To minimise the calculation duration, the crack extension per cycle was computed for a range of a and a/c values and the result for an arbitrary cycle was obtained by interpolation. The R curve behaviour of the coarse grained material A25 has not been taken into account since its effect is not important for the applied thermal loading conditions as it has been previously shown in Ref. [17]. Moreover, no fatigue threshold has been fixed.

Fig. 8 shows the maximum of the SIF at A and C, denoted, respectively, by K_{Amax} and K_{Cmax}, calculated for the A3 alumina as a function of the relative crack depth a/w, for various ratios a/c. It can be seen that over the domain of crack propagation ($0.02 < a/w < 0.1$), K_C is independent of a/c, whereas K_A increases as this ratio decreases.

The use of the SCG law obtained from double torsion or dynamic fatigue tests leads to very small crack growth rates and to cycle numbers that exceed the measured values by several orders of magnitude. Thus, it becomes evident that life time prediction under thermal

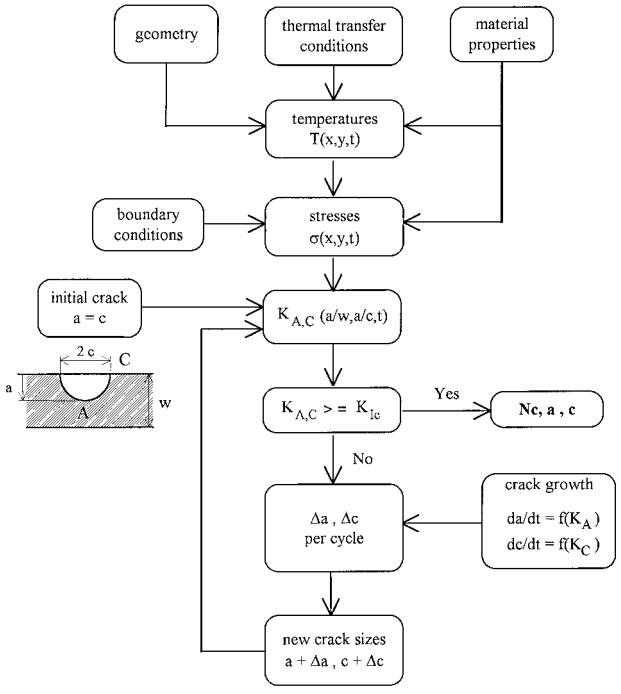

Fig. 7. Flow chart of the thermal fatigue simulation.

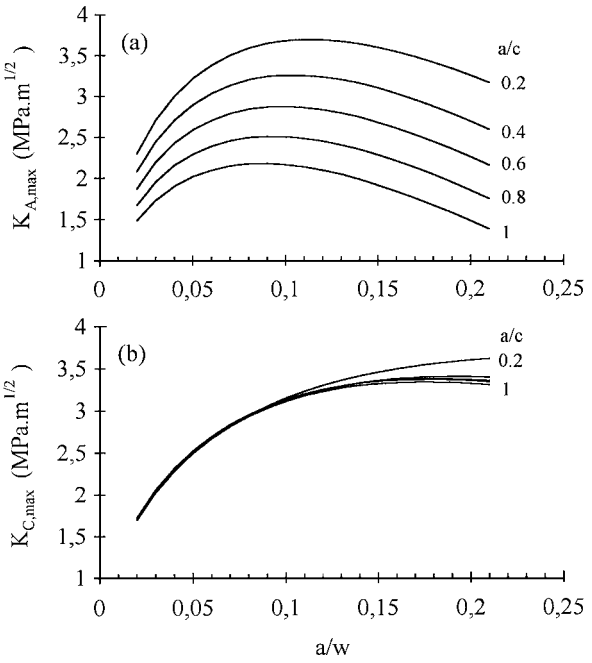

Fig. 8. Maximum stress intensity factor (a) K_{Amax} and (b) K_{Cmax} vs the relative crack depth a/w for various crack aspect ratios a/c.

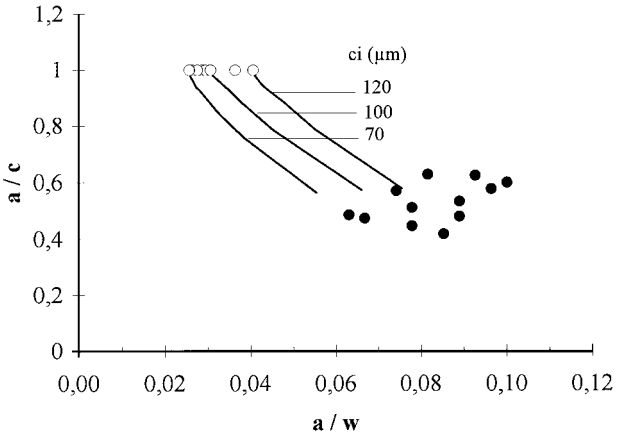

Fig. 9. Evolution of the crack aspect ratio a/c with the relative crack depth a/w as predicted by the simulation for the A3 alumina. The open and the solid symbols denote respectively initial and final measured crack data.

fatigue cannot be based on SCG law from monotonic mechanical loading as it is the case for the glass [18]. In the following, only the results obtained with the law corresponding to the upper limit of the fatigue domain in the $V - K_I$ diagram will be considered.

The evolution of the aspect ratio a/c with the relative crack depth a/w for the fine grain material, A3 is shown in Fig. 9 where the open and solid symbols denote, respectively, the initial and final cracks. The simulation predicts a final aspect ratio a/c of about 0.6 which is in agreement with the measured values. Table 5 shows that the calculated critical cycle numbers are higher than the measured values whereas the total surface crack increment Δc is underestimated by the simulation. This shows that the propagation law used is still approximative according to the simplifications used: only the surface stress has been taken into account and the same propagation law has been used at both the deepest and the surface point of the crack, although a higher propagation at the last point cannot be excluded as it is more exposed to the jet air.

For the coarse grained material A25, the calculated number of cycles N_c is the same order of magnitude that the measured value for the high initial crack sizes ($> 180\,\mu m$) while an important discrepancy is observed for small crack sizes (Table 6). This may be attributed to the following reasons, in addition to those involved above:

1. The range of the critical cycle numbers is not large enough to obtain precise information: within a narrow domain of crack sizes, the unstable crack

Table 5
Measured and calculated values of the crack extensions and the critical cycle number for the A3 alumina

	N_c		Δa(μm)		Δc(μm)	
c_i(μm)	Measured	Calculated	Measured	Calculated	Measured	Calculated
65	>600	800		122		337
76	19	339	180	92	535	221
79	18	218	110	125	310	357
82	14	191	207	220	418	268
85	2	158	182	92	471	221
85	16	158	159	92	304	221
88	8	132	145	111	434	287
91	42	115	109	108	331	277
91	12	115	131	108	298	277
91	12	115	209	108	409	277
108	4	63	170	97	336	238
108	13	63	125	97	348	238
121	3	25	146	106	379	271

Table 6
Measured and calculated critical cycle number for the A25 alumina

c_i(μm)	120	140	150	157	160	171	177	180	185	187	190	194	200	211	212	215	215	215
Nmes	>600	>600	190	40	80	13	18	8	10	10	27	5	20	3	3	3	5	6
Ncal	164		35					11			9		7			5		

growth occurs after a few cycles or after the 600th cycle at which the experiment is stopped. Only the fractured specimens are considered, which limits the extent of the analysis.

2. The indentation cracks are assumed to be initially semi-circular. This assumption was verified for the fine grain material A3 but for the coarse grain material A25, the large indentation load used (100N) may introduce lateral cracking that influences the morphology of the cracks [19,20].

7. Conclusion

The thermal fatigue behaviour of two alumina ceramics is investigated experimentally and analytically. Applying the same temperature difference to specimens containing indentation controlling flaws and plotting the critical cycle number versus the initial crack size allowed the determination of a thermal fatigue domain in the $V - K_I$ diagram.

The crack growth law obtained from the fatigue experiments shows that the life time prediction cannot be made only from the subcritical crack growth behaviour corresponding to isothermal monotonic mechanical loading. Cyclic fatigue effects as well as the temperature variation must be taken into account.

Simulation of the fatigue experiments using the thermal fatigue crack growth law leads to predictions in rather good agreement with the experiments for the fine grain material, but discrepancies are observed for the coarse grain material. For precise investigation, the analysis must be extended to other crack sizes and other applied temperature differences.

References

[1] D.P.H. Hasselman, R. Badaliance, E.P. Chen, Thermal fatigue of materials and components, Proceeding of the symposium, New Orleans, 1975, American Society for Testing and Materials, Philadelphia, 1976, p. 55.
[2] D.P.H. Hasselman, E.P. Chen, C.L. Ammann, J.E. Doherty, C.G. Nessler, J. Am. Ceram. Soc. 58, 11–12 (1975) 513.
[3] N. Kamiya, O. Kamigaito, Thermal fatigue life of glass subjected to air blast quenching, J. Mater. Sci. 14 (1979) 573.
[4] J.P. Singh, K. Niihara, D.P. Hasselman, Thermo-mechanical and thermal behaviour of high temperature structural materials. Interim Report to Office of Naval Research, 1981 Chapter 4.
[5] A.M. Simoneau, Resistance aux chocs thermiques et à la fatigue thermique de céramiques thermomécaniques. Influence des conditions expérimentales. Ph.D. thesis, University of Limoges, France, 1989.
[6] F. Sudreau, C. Olagnon, G. Fantozzi, O. Leclercq, A refined statistical approach for thermal fatigue life prediction, J. Mater. Sci. 27 (5) (1992) 539–546.
[7] T. Fett, K. Keller, J. Kübler, D. Munz, Thermal fatigue of glass, in: Thermal Shock and Thermal Fatigue Behaviour of Advanced Ceramics, G.A. Schneider, G. Petzow, (Eds.), Kluwer Academic, NATO ASI Series, 1993, pp. 383–392.
[8] F. Magerl, G.A. Schneider, G. Petzow, Thermal fatigue and sub critical crack growth in ceramics, in: Thermal Shock and Thermal Fatigue Behaviour of Advanced Ceramics, G.A Schneider, G. Petzow, (Eds.), Kluwer Academic, NATO ASI Series, 1993, pp. 407–418.
[9] F. Mignard, C. Olagnon, G. Fantozzi, Thermal fatigue—comparison with theoretical prediction, in: Fracture Mechanics of Ceramics, Vol. 11, R.C. Bradt, D.P.H. Hasselman, D. Munz, M. Sakai, V. Ya. Shevchenko, (Eds.), Plenum Press, New York, 1996, pp. 45–60.
[10] E.D. Case, Y. Kim, W.J. Lee, Cyclic thermal shock in SiC whisker reinforced alumina and in other ceramic systems, in: Thermal Shock and Thermal Fatigue Behaviour of Advanced Ceramics, G.A Schneider, G. Petzow, (Eds.), Kluwer Academic, NATO ASI Series, 1993, pp. 393–406.
[11] K.J. Konsztowicz, Acoustic emission amplitude analysis in crack growth studies during thermal shock of ceramics, in: Thermal Shock and Thermal Fatigue Behaviour of Advanced Ceramics, G.A Schneider, G. Petzow, (Eds.), Kluwer Academic, NATO ASI Series, 1993, pp. 429–441.
[12] F. Mignard, C. Olagnon, G. Fantozzi, P. Chantrenne, M. Raynaud, Thermal shock behaviour of a coarse grain porous alumina, J. Mater. Sci. 13 (1996) 2131–2138.
[13] D.P. Williams, A.G. Evans, A simple method for studying slow crack growth, J. Testing and Evaluation 1 (4) 264–270.
[14] R.J. Charles, Dynamic fatigue of glass, J. Appl. Phys. 29 (9) (1958) 1657–1661.
[15] J. Chevalier, M. Saadaoui, C. Olagnon, G. Fantozzi, Double-torsion testing of a 3Y–TZP ceramic, Ceramics, International 22 (1996) 171–177.
[16] K. Jakus, D.C. Coyne, J.E. Ritter, Analysis of fatigue data for lifetime predictions for ceramic materials, J. Mater. Sci. 13 (1978) 2071–2080.
[17] M. Saadaoui, G. Fantozzi, Crack growth resistance under thermal shock loading of alumina. Mater. Sci. Eng. A247 (1998) 142–151.
[18] T. Fett, K. Keller, D. Munz, Subcritical crack gowth in borosilicate glass under thermal fatigue, Theor. Appl. Frac. Mech. 16 (1991) 27–34.
[19] B.R. Lawn, A.G. Evans, D.B. Marshall, Elastic/plastic indentation damage in ceramics: the median/radian crack system, J. Am. Ceram. Soc 63 (9–10) (1980) 574–581.
[20] R.F. Cook, E.G. Liniger, R.W. Steinbrech, F. Deuerler, Sigmoidal indentation strength characteristics of polycrystalline alumina, J. Am. Ceram. Soc 77 (2) (1994) 303–314.